CO_2 hydrate formation in aqueous solutions: Phase field theory of nucleation and growth

L. Gránásy,[†] T. Pusztai,[†] G. Tegze,[†] T. Kuznetsova,[‡] B. Kvamme[‡]

[†]*Research Institute for Solid State Physics and Optics, H-1525 Budapest, POB 49, Hungary*
[‡]*Department of Physics, University of Bergen, Allégaten 55, N-5007 Bergen, Norway*

Abstract A phase field theory developed recently [Gránásy, L; Börzsönyi, T.; Pusztai, T. Phys. Rev. Lett. 2002, 88, 206105] is applied to describe the formation of CO_2 hydrate in aqueous solutions. Starting from realistic estimates for the thermodynamic and interfacial properties, we show that under typical conditions of CO_2 formation, the size of the critical fluctuations (nuclei) is comparable to the interface thickness, implying that the classical droplet model, which relies on a sharp interface, is rather inaccurate. The phase field theory predicts considerably smaller nucleation barrier than the classical approach and converges, as expected, to the classical prediction with decreasing interface thickness. We determine the dimensionless growth rate of small CO_2 hydrate clusters in aqueous solution. Finally, we explore the possibility to model solidification in porous matter and liquid channel using the phase field theory.

Introduction

The amount of carbon bound in natural gas hydrates is conservatively estimated to be twice the amount of carbon to be found in fossil fuels on Earth [1]. Assuming that the lattice is filled to the maximum capacity, 1 m^3 gas hydrate may release about 164 m^3 methane under standard temperature and pressure condition [2]. CO_2 hydrate is significantly more stable thermodynamically than methane hydrate. Storage of CO_2 in hydrate reservoirs through replacement of natural gas is therefore considered as an interesting option for safe long terms storage of CO_2, which can be economically feasible due to the produced natural gas. The efficiency of any exploitation strategy based on CO_2 depends on the composite dynamics of the system, where knowledge of the kinetics of hydrate reformation is crucial. Storage of CO_2 is in aquifers is another option for reducing CO_2 emissions to the atmosphere. This option is already in use outside the coast of Norway, where CO_2 from the Sleipner field is being injected into the Utsira formation. Similar storage option may be used outside the Northern part of Norway. In these regions the seabed temperature may be as low as – 1 $^{\circ}$C and substantial regions of the reservoirs may be inside the hydrate stability zones. Therefore, hydrate may form homogeneously from dissolved CO_2 or at the interface between free CO_2 and water.

Development of the related technologies requires a detailed understanding of all processes involved, a knowledge that can be gained by combined experimenting and modeling. An essential ingredient of such an approach is the development of appropriate theoretical tools that can describe quantitatively all stages of the processes involved. A little understood step of hydrate formation is nucleation, in which nanometer sized hydrate crystallites form via thermal fluctuations.

In this paper, we apply the phase field theory for describing the nucleation and growth of CO_2 hydrate under conditions specific to underwater reservoirs. The phase field theory (PFT) is one of the most potent methods for modeling solidification in binary, ternary and multi-component melts. The ability of the PFT to describe complex solidification morphologies has been demonstrated over the past decade [3]. This includes the thermal and solutal dendrites [4-6], the eutectic/peritectic fronts [8-10], and crystal nucleation in alloys [11,12]. It has been shown that for systems where the input parameters of the PFT are known with satisfactory accuracy, it predicts the nucleation rate with a considerably better accuracy than the sharp interface droplet model of the classical theory that, in turn, fails by several orders of magnitude. We are going to show that using reasonable input data, similar differences occur in the case of hydrate formation. We predict the growth rate of hydrate particles and we address problems associated with freezing in the presence of walls including solidification in porous medium and channels.

Models for nucleation and growth

The freezing of homogeneous undercooled liquids starts with the formation of heterophase fluctuations whose central part shows crystal-like atomic arrangement. Those heterophase fluctuations that exceed a critical size (determined by the interplay of the interfacial and volumetric contributions to the cluster free energy) have a good chance to reach macroscopic dimensions, while the smaller ones decay with a high probability. (Heterophase fluctuations of the critical size are called *nuclei*.) The description of the near-critical fluctuations is problematic even in single component systems. The main difficulty is that the typical size of the critical fluctuations, forming on the human time scale, is about 1 nm, comparable to the thickness of the crystal-liquid interface, which in turn extends to several molecular layers [13]. Therefore, the droplet model of the classical nucleation theory, which relies on a sharp interface and bulk crystal properties, is inappropriate for such fluctuations. Field theoretic models, that predict a diffuse interface, offer a natural way to handle such a situation [14]. For example, in recent works, the phase field theory has been shown to describe such fluctuations quantitatively [11,12,15].

Phase field theory of nuclei

Our starting point is the standard phase field theory of binary alloys as developed by several authors [6,16]. In the present approach, the local state of the matter is characterized by two fields; a structural order parameter, ϕ, called the *phase field*, that describes the transition between the disordered liquid and ordered crystalline structures, and a conserved field, the coarse-grained solute concentration, c.

The structural order parameter can be viewed as the Fourier amplitude of the dominant density wave of the time averaged singlet density in the solid. As pointed out by Shen and Oxtoby [17] if the density peaks in the solid can be well approximated by Gaussians placed to the atomic sites, all Fourier amplitudes can be expressed uniquely in terms of the amplitude of the dominant wave, thus a single structural order parameter suffices. Here we take $m = 0$ in the solid and $m = 1$ in the liquid. We assume mass conservation, which implies that the integral of the conservative fields over volume is a constant.

The free energy of the system is a functional of these fields:

$$F = \int d^3r \left\{ \tfrac{1}{2}\varepsilon^2 T(\nabla m)^2 + f(m,c) \right\}, \tag{1}$$

where ε is a constant, T is the temperature, and $f(m,c)$ is the local free energy density. The first term on the right hand side is responsible for the appearance of the diffuse interface. The local free energy density has the form $f(m, c) = wT\, g(m) + [1 - p(m)]\, f_S(c) + p(m)\, f_L(c)$, where the "double well" and "interpolation" functions have the forms $g(m) = {}^1\!/_4\, m^2(1 - m)^2$ and $p(m) = m^3(10 - 15m + 6m^2)$, respectively, that emerge from the thermodynamically consistent formulation of the PFT [18], w is the free energy scale, while the free energy densities of the homogeneous solid and liquid, f_S and f_L, depend on the local value of c. These relationships result in a free energy surface that has two minima, whose relative depth depends on the deviation from equilibrium.

Being in unstable equilibrium, the critical fluctuation (the nucleus) can be found as an extremum of this free energy functional [11,12,14,15,19], subject to the solute conservation constraint discussed above. To impose this constraint one adds the volume integral over the conserved field times a Lagrange multiplier, λ, to the free energy: $\lambda \int d^3r\, c(\mathbf{r})$. The field distributions, that extremize the free energy, have to obey the appropriate Euler-Lagrange (EL) equations, which in the case of such local functional take the form

$$\frac{\delta F}{\delta m} = \frac{\partial \psi}{\partial m} - \nabla \frac{\partial \psi}{\partial \nabla m} = 0$$

$$\frac{\delta F}{\delta c} = \frac{\partial \psi}{\partial c} - \nabla \frac{\partial \psi}{\partial \nabla c} = 0 \tag{2}$$

where $\delta F/\delta m$ and $\delta F/\delta c$ stands for the first functional derivative of the free energy with respect to the fields m and c, respectively while ψ is the total free energy density. The EL equations have to be solved assuming that unperturbed liquid exists in the far field, while, for symmetry reasons zero field gradients exist at the center of the fluctuations. Under such conditions, the Lagrange multiplier can be identified as $\lambda = -(\partial\psi/\partial c)_{r\to\infty}$.

Assuming spherical symmetry that is reasonable considering the low anisotropy of the crystal-liquid interface at small undercoolings, the EL equations take the following form:

$$\varepsilon^2 T\left\{\frac{d^2m}{dr^2}+\frac{2}{r}\frac{dm}{dr}\right\} = wTg'(m)+p'(m)\{f_L - f_S\}, \tag{3a}$$

and

$$0 = wTg(m)+\left[1-p(m)\right]\frac{\partial f_S}{\partial c}+p(m)\frac{\partial f_L}{\partial c}-\left.\frac{\partial f_L}{\partial c}\right|_{r\to\infty}. \tag{3b}$$

Here $'$ stands for differentiation with respect to the argument of the function. The last term in eqn. (3b) originates from the Lagrange multiplier. Since the right hand side of eqn. (3b) is a function of fields c and m, it provides the implicit relationship $c = c(m)$. Accordingly, eqn. (3a) is an ordinary differential equation for $m(r)$. This equation has been solved here numerically using a fourth order Runge-Kutta method. Since m and dm/dr are fixed at different locations, the central value of m that satisfies $m \to m_\infty = 1$ for $r \to \infty$, has been determined iteratively. Having determined the solutions $m(r)$ and $c(r)$, the work of formation of the nucleus W^* can be obtained by inserting the solution into the free energy functional. Provided that the bulk free energy densities, $f_S(c)$ and $f_L(c)$, are known, the only model parameters, we need to fix to evaluate W^*, are w and ε. These model parameters are related to the interface thickness and the interfacial free energy [6,19], thus these quantities can be used to determine w and ε, and calculate W^* *without adjustable parameters*.

The steady state nucleation rate (number of nuclei formed in unit volume and time), J_{SS}, can be calculated as

$$J_{SS} = J_0 \exp\left\{-W^*/kT\right\}, \tag{4}$$

using the classical nucleation prefactor [20], J_0, verified experimentally on oxide glasses [21].

Classical droplet model (CDM) of nuclei

For comparison with the phase field theory, we calculate the height of the nucleation barrier using the sharp interface droplet model of the classical nucleation theory. In this approach, the free energy of heterophase fluctuations of radius R is given as $W_{CDM} = -(4\pi/3)R^3\Delta g + 4\pi R^2\Gamma_\infty$, where $\Delta g = \rho(\mu_L - \mu_S)$ is the volumetric Gibbs free energy difference between the bulk liquid and solid, μ_L and μ_S are the chemical potential of the liquid and the solid, and Γ_∞ is the free energy of the equilibrium planar interface. Then, the free energy of the critical fluctuation of radius $R^*_{CDM} = 2\Gamma_\infty/\Delta g$ is $W^*_{CDM} = (16\pi/3)\,\Gamma_\infty^3/\Delta g^2$. These results are expected to be accurate when the interface is thin relative to the radius of the critical fluctuation, $d \varsigma R$.

Phase field theory of polycrystalline growth

To address hydrate crystallization and polycrystalline growth, we rely on an extension of the phase field theory developed recently [11,12,22], which relies on the orientation field, θ, first introduced by Kobayashi, Warren and Carter [23]. This field specifies the local orientation of the crystal planes in the laboratory system, and allows the description of polycrystalline solidification and grain boundary evolution. It normalized so that it varies between 0 and 1, while the orientation angle covers 0 and $2\pi/n$, where n is the symmetry index (e.g., $n = 6$ applies for six-fold symmetry). In order to handle nucleation of crystallites with different crystallo-

graphic orientations, we assume that θ fluctuates in space and time. This extension of the orientation field to the liquid phase captures the short-range order existing in the liquid. The orientation field is strongly coupled to the phase field so that structural and orientational changes take place simultaneously at the crystal-liquid interface. This coupling is realized by adding an orientational contribution to the free energy functional.

$$F = \int d^3r \left\{ \tfrac{1}{2}\varepsilon^2 T(\nabla m)^2 + f(m,c) + f_{ori}(m,\nabla\theta) \right\}, \tag{5}$$

where $f_{ori}(m, \nabla\theta) = [1 - p(m)]HT\left|\nabla\theta\right|$ is the driving force for orientational ordering, and H is a constant.

The equations of motion for the three fields are

$$\begin{aligned}
\dot{\phi} &= -M_m \frac{\delta F}{\delta m} = M_m \left\{ \nabla\left(\frac{\partial f}{\partial \nabla m} \right) - \frac{\partial f}{\partial m} \right\} + \zeta_m \\
\dot{c} &= \nabla M_c \nabla \frac{\delta F}{\delta c} = \nabla \left\{ Dc(1-c)\nabla \left[\left(\frac{\partial f}{\partial c} \right) - \nabla\left(\frac{\partial f}{\partial \nabla c} \right) \right] \right\} + \zeta_j \\
\dot{\theta} &= -M_\theta \frac{\delta F}{\delta \theta} = M_\theta \left\{ \nabla\left(\frac{\partial f}{\partial \nabla \theta} \right) - \frac{\partial f}{\partial \theta} \right\} + \zeta_\theta
\end{aligned} . \tag{6}$$

Here ζ_i ($i = m, j, \theta$) are Langevin noise terms for the two non-conserved fields m and θ, and for the concentration flux j, that model the thermal fluctuations in the system. Introducing the time scale $\tau = \xi^2 / D_l$, where ξ is a length scale and D_l the diffusion coefficient of the liquid, the following dimensionless forms emerge for the deterministic part of the equations of motion:

$$\tilde{\dot{m}} = \frac{M_m \varepsilon^2 T}{D_l} \left[\begin{aligned} &\tilde{\nabla}(s^2 \tilde{\nabla} m) - \frac{\partial}{\partial \tilde{x}} \left\{ s \frac{\partial s}{\partial \vartheta} \frac{\partial m}{\partial \tilde{y}} \right\} + \frac{\partial}{\partial \tilde{y}} \left\{ s \frac{\partial s}{\partial \vartheta} \frac{\partial m}{\partial \tilde{x}} \right\} \\ &\qquad - \xi^2 \frac{w(c)Tg'(m) + p'(m)\left\{ f_L(c,T) - f_S(c,T) - HT\left|\tilde{\nabla}\theta\right| / \xi \right\}}{\varepsilon^2 T} \end{aligned} \right]$$

$$\tilde{\dot{c}} = \tilde{\nabla} \left\{ \frac{v_m}{RT} \lambda c(1-c) \tilde{\nabla} \left[\begin{aligned} &(w_B - w_A)Tg(m) + [1 - p(m)] \frac{\partial f_S}{\partial c}(c,T) \\ &+ p(m) \frac{\partial f_L}{\partial c}(c,T) \end{aligned} \right] \right\}$$

$$\tilde{\dot{\theta}} = \chi \left[\tilde{\nabla} \left\{ [1 - p(m)] \frac{\tilde{\nabla}\theta}{\left|\tilde{\nabla}\theta\right|} \right\} - \frac{\varepsilon^2}{H\xi} s \frac{\partial s}{\partial \theta} \left|\tilde{\nabla}\phi\right|^2 \right] .$$

where tilde denotes differentiation with respect to dimensionless quantities. Here $M_c = (v_m/RT)\, D\, c\, (1 - c)$ is the mobility of the concentration field, v_m the average molar volume, $D = D_s + (D_l - D_s)\, p(m)$ is the diffusion coefficient, and $\lambda = D / D_l$ is the reduced diffusion coefficient is, while $\chi = M_\theta\, \xi\, HT / D_l$ is the dimensionless orientational mobility. Note a second term on the RHS of the equation for the orientation field included recently [24].

In this work, these equations were solved numerically using an explicit scheme and MPI protocol on a PC cluster consisting of 56 nodes, built up in the Research Institute for Solid State Physics and Optics, Budapest. A periodic boundary condition is applied at the borders of the simulation window, unless stated otherwise.

To study solidification in a confined space, we introduce "walls", where the normal component of ∇m and ∇c are set zero ("no flux" boundary condition). The former ensures a 90 degrees contact angle, while the latter realizes a chemically inert wall.

Material properties

The molar Gibbs free energy of the aqueous CO_2 solution has been calculated as $G_L = (1 - c)\, G_{L,W} + c\, G_{L,CO2}$, where c is the mole fraction of CO_2. The partial molar Gibbs free energy of water in solution has been obtained as $G_{L,W} = G_{L,W}^0 + RT \ln[(1 - c)\, \gamma_{L,W}(c)]$, where the free energy of pure water has been calculated as

$$G_{L,W}^{\ 0} = \sum_{i=0}^{3} \frac{k_i}{T^i}\,, \tag{7}$$

with coefficients k_i taken from Ref. 25. Here R is the gas constant and $\gamma_{L,W}$ is the activity coefficient of water in solution. The partial molar free energy of CO_2 in solution is $G_{L,CO2} = G_{L,CO2}^{\infty} + RT \ln[c\, \gamma_{L,CO2}(c)]$, where the molar free energy of CO_2 at infinite dilution, $G_{L,CO2}^{\infty} = -19.67$ kJ/mol, has been taken from molecular dynamics simulations [26]. The temperature and pressure dependent activity coefficient of CO_2 in aqueous solution deduced from CO_2 solubility experiments of Stewart and Munjal [27] have been fitted using the form

$$\ln \gamma_{L,CO_2} = \sum_{i=0}^{5} a_i(T) \left[\ln x\right]^i\,, \tag{8}$$

with $a_i(T)$ given by third order polynomials. The activity coefficient of water, $\gamma_{L,W}$ in aqueous solution has been obtained from eqn. (6) via the Gibbs-Duhem relationship.

The Gibbs free energy of the hydrate is given by $G_S = (1 - c)G_{S,W} + cG_{S,CO2}$. Owing to the lack of experimental information, the partial molar quantities have been calculated using the model described in Ref. 25. For water and CO_2 we use the relationships $G_{S,W} = G_{S,W}^0 + RT\ (3/23)\ \ln(1 - \theta)$, and $G_{S,CO2} = G_{S,CO}^{inc} + RT \ln[\theta/(1 - \theta)]$, respectively, where the hole occupancy is $\theta = c/(3/23)$. Here, the partial molar Gibbs free energies of the empty clathrate, $G_{S,W}^0$, and that of guest inclusion, $G_{S,CO}^{inc}$, are given by eqn. (6), with the appropriate k_i taken from Ref. 25.

Following other authors [28], we approximate the free energy of the hydrate-solution interface by that of the ice-water interface, taken from the work of Hardy, 29.1 ± 0.8 mJ/m^2 [29]. This is in good agreement with recent experimental data for the CO_2 hydrate system (~30 mJ/m^2), we became aware recently [30]. Owing to a lack of information on the CO_2 hydrate/aqueous solution interface, we use the 10% – 90% interface thickness, d, (the distance on which the phase field changes between 0.1 and 0.9) as an adjustable parameter in the calculations. Molecular dynamics simulations on other clathrate hydrates indicate that the full interface thickness is about 2 – 3 nm [31], that corresponds to roughly $d \approx 1 - 1.5$ nm. Assuming that similar values apply for the CO_2 hydrate, we vary d in the 0.125 – 1.5 nm range. Indeed MD simulations of the melting of CO_2 hydrate, performed at the University of Bergen, indicate d in the same range, although a dynamic broadening of the interface cannot be excluded (Fig. 1).

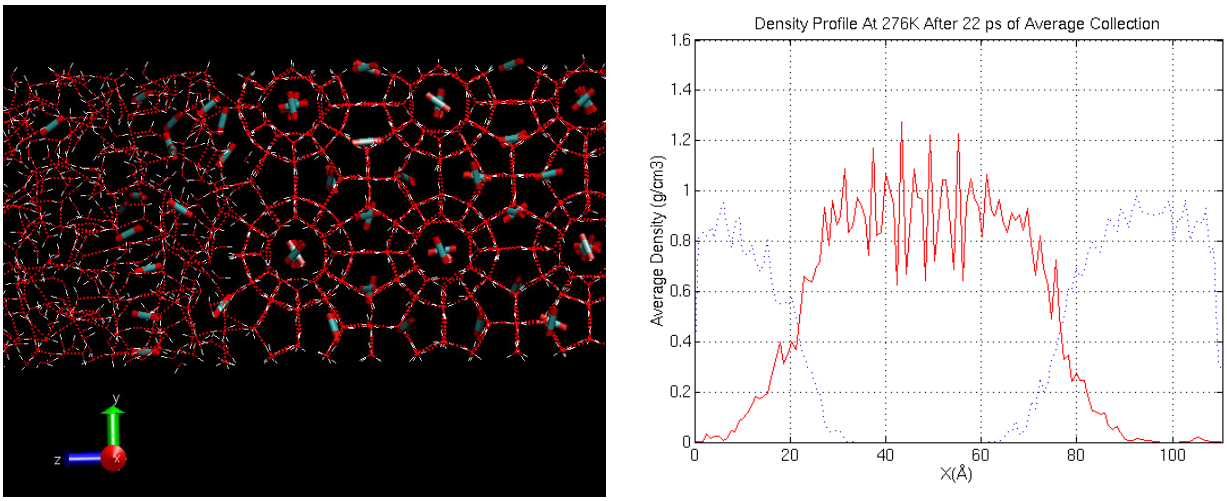

Fig. 1 Snapshot of a molecular dynamics simulation on the melting of CO_2 hydrate in the presence of water and the interface liquid (blue) and hydrate (red) densities. The simulation consists of 920 water and 108 CO_2 molecules (represented by SPC and EPM2 potentials, respectively), and has been performed at 276.15 K and 200 Bar. Note the regular clathrate cages inside the solid (on the right) and the distorted cages at the interface (on the left). The diameter of the H_2O cages of circular projection (tetrakaidecahedra) is 0.866 nm. The rods at the center of the cages denote the CO_2 molecules. [This picture have been made using the Visual Molecular Dynamics package (Humphrey, W.; Dalke, A.; Schulten, K. J. Molec. Graphics, 1996, 14, 33).]

The computations are performed under conditions typical for the seabed reservoirs, i.e. $T = 274$ K, $p = 15$ MPa (~ 1500 m depth), furthermore, we assume that water has been saturated by CO_2 ($c = 0.033$, obtained by extrapolating the relevant data by Teng and Yamasaki [32]). These experimental data are for synthetic average seawater. The salinity of groundwater in reservoirs may vary from close to zero up to seawater salinity in regions where the penetration of seawater dominates the salinity.

In the 2D phase field simulations for CO_2 hydrate we used $\varepsilon^2 = 1.3944 \times 10^{-15}$ J/cm K, $w = 3.6372$ J/cm^{3}K, $D_l = 10^{-5}$ cm^2/s, $D_s = 0$, $\xi = 10^{-8}$ cm, $m_m = M_m\varepsilon^2 T/ D_l = 4.4308$, and $\chi = 0.8381$, while the time and spatial steps were $\Delta t = 0.04\ \tau$ and $\Delta x = \xi$, respectively. Simulations for confined space were done for Ni-Cu, using the properties given in previous works of us [11,12].

Results

Hydrate nucleation

The free energy surface, corresponding to ε and w that reproduce the ice-water interface free energy and a 10% – 90% thickness of 1 nm at $T = 274$ K, is shown in Fig. 2. The radial structural order parameter and concentration profiles of the critical fluctuations forming in saturated aqueous CO_2 solution ($c = 0.033$) at the same temperature are shown in Fig. 3 as a function of the interface thickness, d.

Remarkably, at the realistic interface thickness ($d = 1.0$ to 1.5 nm) the bulk crystalline structure is not yet established even at the center of the nucleus, indicating that the nucleus is softer (the molecules have larger amplitude of oscillations around the crystal sites) than the bulk crystal. Despite these, we have almost full hole-occupancy in the central part, $c = 0.1235$ or $\theta = 0.946$. Furthermore, the interface thickness for the concentration field is far sharper than for structure. It extends to only a few Å, which is consistent with the picture that the nucleus is a small piece of hydrate crystal embedded into the solution, however, built of somewhat distorted H_2O cages seen at the interface in MD simulations with realistic potentials (Fig. 1) [33]. It is remarkable, that the interface for the solute falls close to the classical radius $R^*_{CDM} = 1.76$ nm.

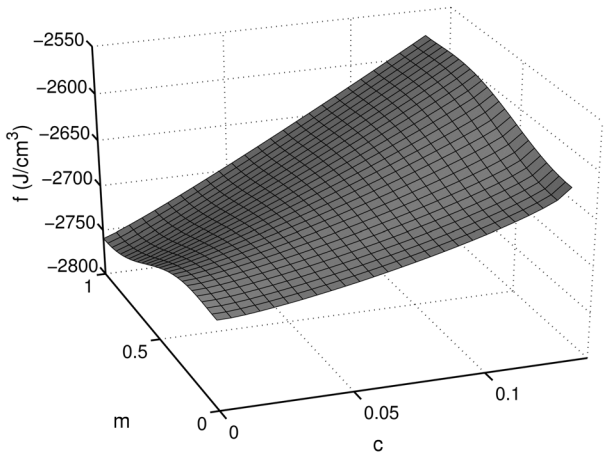

Fig. 2 Free energy density surface for the CO_2 hydrate system at 274 K, evaluated with free energy scale w corresponding d = 1 nm and $\Gamma_\infty = 29.1 \pm 0.8$ mJ/m^2. (m – phase field, c – mol fraction of CO_2.)

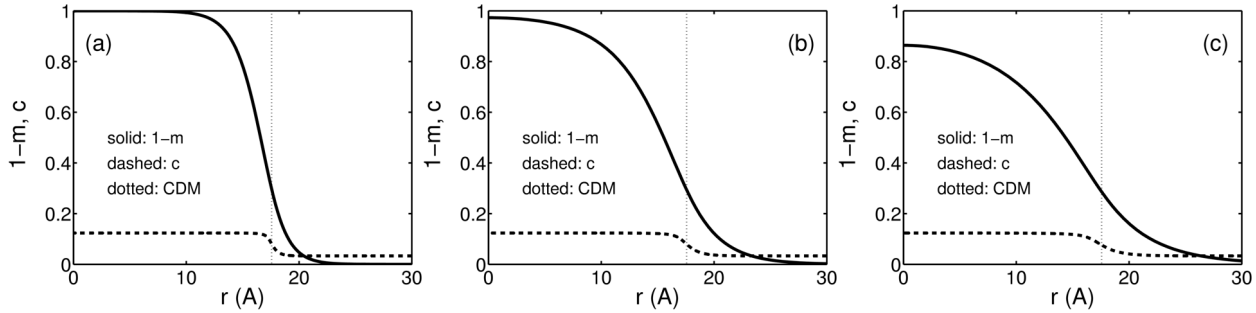

Fig. 3 Radial 1 − m profiles (solid lines) and CO_2 concentration profiles (dashed lines) for critical fluctuations calculated at T = 274 K, for 10% − 90% interface thickness d = (a) 0.5, (b) 1.0 and (c) 1.5 nm. For comparison the critical radius from the CDM is also shown (dotted vertical lines).

In agreement with previous studies on other systems [11,12,15], a substantial difference can be seen between predictions made for the height of the nucleation barrier by the phase field theory and the classical droplet model (Table 1). This difference emerges from the fact that the interface thickness is comparable to the size of the critical fluctuation. As one should expect, for decreasing interface thickness, the PFT prediction for the height of the nucleation barrier converges to that by the sharp interface CDM ($W^*_{\mathrm{PFT}} \to W^*_{\mathrm{CDM}}$ for $d \to 0$; see Fig.4), indicating the coherency of our results. These findings imply that, similarly to many other systems, in hydrate forming systems the classical droplet model of crystal nuclei is rather inaccurate and should be replaced by more advanced approaches such as the phase field theory.

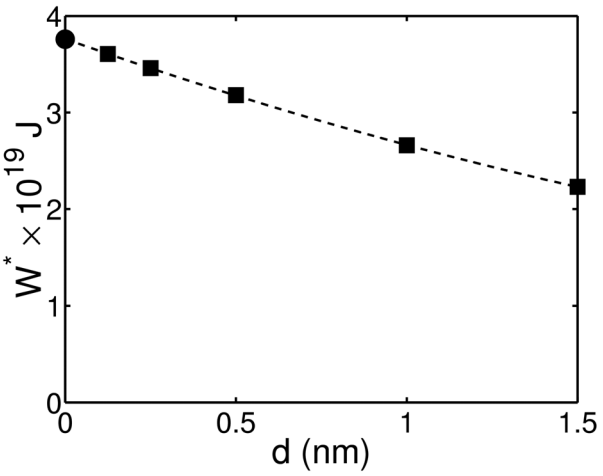

Fig. 4 Height of the nucleation barrier for CO_2 hydrate formation as a function of interface thickness in the phase field theory (squares). For comparison, the prediction of the classical droplet model that assumes a sharp interface (d = 0) is also presented (circle).

Table 1 Free energy of critical fluctuations (W^*) vs. the interface thickness in the CO_2 hydrate system, as predicted by the phase field theory (PFT) and the classical droplet model (CDM) at 274 K and c = 0.033.

d (nm)	$W^*_{PFT}(10^{-19}$ J)	$W^*_{CDM}(10^{-19}$ J)
0.125	3.61	
0.25	3.46	
0.5	3.18	
1.0	2.66	3.76
1.5	2.23	

The temperature and composition dependencies of the free energy of nuclei are shown for both cluster models in Fig. 5 (in the case of PFT d = 1 nm is assumed). With decreasing temperature and increasing mole fraction of CO_2 dissolved in water, the height of the nucleation barrier decreases, leading to enhanced nucleation rate.

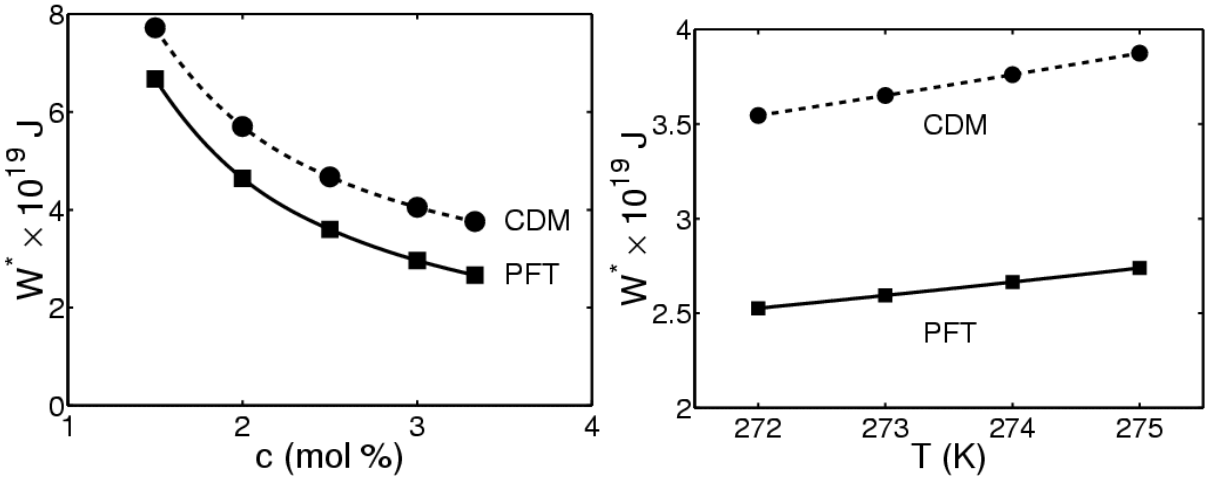

Fig. 5 Left: Height of the nucleation barrier for CO_2 hydrate formation as a function of composition (left) and temperature (right) in the phase field theory (squares) and the classical droplet model (circles).

We note, that the predicted W^* is rather sensitive to the values of Γ_∞ and d used to fix the model parameters ε and w. Thus, accurate results may only be expected if these input properties are known with a high accuracy. Unfortunately, none of them is available for the CO_2 hydrate/solution interface (the values used here and in other work [28] are only rough estimates). Therefore, further effort is needed to establish accurate nucleation rates. For example, careful experiments using the grain boundary groove method [29] could provide a reasonably accurate value for the interfacial free energy. Another possible way to determine the interfacial properties is via MD simulations [13,34] with realistic interaction potentials. Work is underway in these directions.

Growth of CO_2 hydrate particles

The growth of a supercritical CO_2 hydrate particle is shown in Fig. 6. Maps of the three fields and the radial phase field and concentration profiles are presented. Note a CO_2 depletion zone ahead of the solidification front (Fig. 6a), which is responsible for the diffusion governed slowing down of growth. The radius of the particle (defined by the position where $m = 0.5$) is presented as a function of time in Fig. 7. The time-dependence indicates that, as expected, growth is governed here by CO_2 diffusion in the liquid.

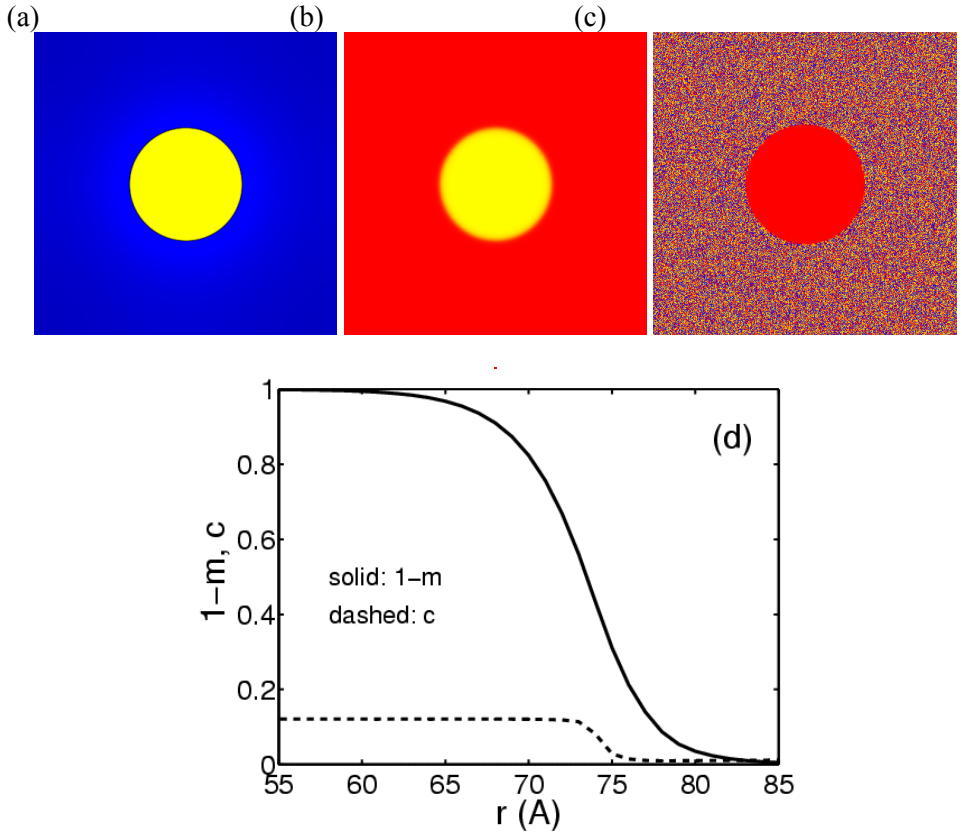

Fig. 6 Growth of a supercritical [R (t = 0) = 2.5 nm] CO_2 hydrate particle in saturated aqueous solution at 274 K and 15 MPa in the phase field theory (d = 1.0 nm, isotropic case). (a) Composition map (aqueous solution – blue, hydrate – yellow); (b) phase field map (solid – yellow, liquid – red); (c) orientation field (different colors denote different orientations). (d) Radial phase field and composition field profiles. The growth shapes are shown after 94 ns. The computations refer to a 40 × 40 nm area.

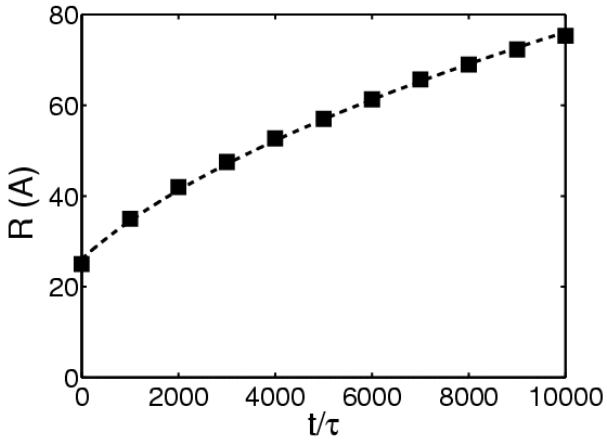

Fig. 7 Radius of the CO_2 particle as a function of reduced time during the early growth stage in 2D. (Here $\tau = 10^{-11}$ s.) Dashed line denotes an $R = [A\ (t - t_0)]^{1/2}$ function fitted to the R(t) relationship [$A = (0.51 \pm 0.01) \times 10^{-5}$ cm^2/s and $t_0 = (-1328 \pm 58) \times 10^{-11}$ s]. The average growth rate for the period shown is ~ 5.3 cm/s. Growth rate, however, slows down as $v = (1/2)[A / (t - t_0)]^{1/2}$, yielding ~ 11 μm/s after 1 s, unless interaction with other particles or the morphological instability intervenes.

Crystal growth in the presence of walls

A recent experimental work addresses hydrate formation in aqueous solution in porous media and rectangular channels [30]. To study solidification in such confined spaces, we introduced walls into the PFT simulations. In our model, the "no-flux" boundary condition is used to realize a rectangular contact angle and a chemically inert wall. In the simulations, the orientation field can be either random [no preferred orientation (glassy wall)] or one may chose preferred orientation(s). The introduction of such walls allows the study of heterogeneous crystal nucleation on particles, rough surfaces, and crystallization in porous matter or in channels. Preliminary results obtained with ideal solution thermodynamics (Ni-Cu system) in the PFT are shown in Figs. 8, 9 and 10. The observed morphologies resemble closely to those seen during hydrate formation in porous matter and in rectangular channels [30]. A similar approach will be used in the future for a quantitative modeling of hydrate formation in confined geometries.

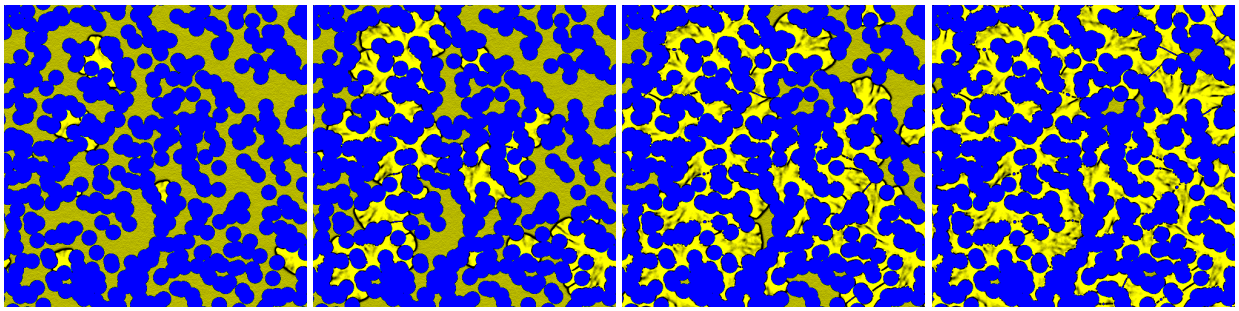

Fig. 8 Solidification in porous matter. Blue – particles of porous matter, dark yellow – liquid, bright yellow – solid.

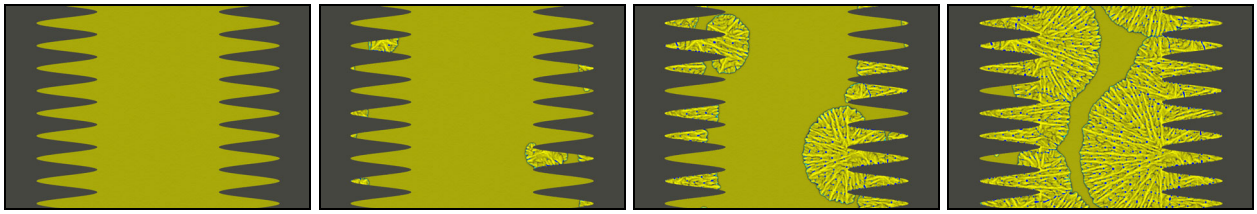

Fig. 9 Heterogeneous nucleation on rough (sinusoidal) surface. Gray – wall, dark yellow – liquid, bright yellow – solid.

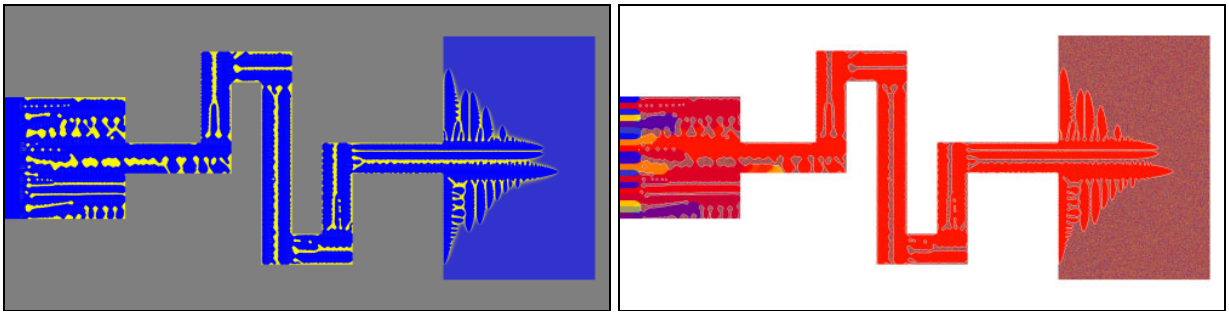

Fig. 10 Dendritic solidification in rectangular channel. Upper panel: composition map (blue – solidus, yellow – liquidus). Lower panel: orientation map (different colors stand for different crystal orientation). Note that a single orientation has been selected.

Conclusions

The nucleation and growth of CO_2 hydrate in aqueous solution is addressed using a phase field theory we developed recently. It has been demonstrated under typical conditions, that the thickness of the hydrate-solution interface is comparable with the size of nuclei, implying that the classical droplet model is rather inaccurate. Indeed, as found for many other systems [11,15], the nucleation barriers predicted by the phase field theory and the classical droplet model differ considerably. Apparently, advanced models are needed to evaluate the rate of hydrate nucleation accurately. The phase field theory is used to predict the growth rate of CO_2 hydrate in aqueous solution. The growth is governed by CO_2 diffusion in the liquid. We have introduced walls into the phase field simulations and demonstrated the possibility for modeling solidification in confined space (channels/porous media).

Acknowledgments

This work has been supported by the Hungarian Academy of Sciences under contract No. OTKA-T-037323 and by the Norwegian Research Council under project Nos. 153213/432 and 151400/210. T. P. acknowledges support by the Bolyai János Scholarship of the Hungarian Academy of Sciences.

References

(1) Milich, L. Global Environmental Change-Human and Policy Dimensions, 1999, 9, 179.
(2) Mienert, J.; Andreassen, K.; Posewang, J.; Lukas, D. Ann. N. Y. Acad. Sci., 2000, 912, 200.
(3) Boettinger, W. J.; Warren, J. A.; Beckermann, C.; Karma, A. Ann. Rev. Mater. Res., 2002, 32, 163.
(4) Kobayashi, R. Physica D, 1993, 63, 410.
(5) Karma, A.; Rappel, W.-J. Phys. Rev. E, 1998, 57, 4323.
(6) Warren, J. A.; Boettinger, W. J. Acta Metall. Mater., 1995, 43, 689.
(7) Karma, A. Phys. Rev. E, 1994, 49, 2245.
(8) Drolet, F.; Elder, K. R.; Grant. M.; Kosterlitz, J. M. Phys. Rev. E, 2000, 61, 6705.
(9) Nestler, B.; Wheeler, A. A. Physica D, 2000, 138, 114.
(10) Lo, T. S.; Karma, A.; Plapp, M. Phys. Rev. E, 2001, 63, 031504.
(11) Gránásy, L.; Börzsönyi, T.; Pusztai, T. Phys. Rev. Lett., 2002, 88, 206105.
(12) Gránásy, L.; Börzsönyi, T.; Pusztai, T. J. Cryst. Growth., 2002, 237-239, 1813.
(13) Davidchack, R. L.; Laird, B. B. J. Chem. Phys., 1998, 108, 9452.
(14) Oxtoby, D. W. Annu. Rev. Mater. Res., 2002, 32, 39.
(15) Gránásy, L.; Pusztai, T.; Tóth, G.; Jurek, Z.; Conti, M; Kvamme, B. J. Chem. Phys. 2003, 119, 10376.

(16) Caginalp, G.; Jones, J. Ann. Phys. (N.Y.), 1995, 237, 66.
(17) Shen, Y. C.; Oxtoby, D. W. J. Chem. Phys., 1996, 105, 6517.
(18) Wang, S. L.; Sekerka, R. F.; Wheeler, A. A.; Murray, B. T.; Coriell, S. R.; Braun, R. J.; McFadden, G. B. Physica D, 1993, 69, 189.
(19) Cahn, J. W.; Hilliard, J. E. J. Chem. Phys, 1958, 28, 258; 1959, 31, 688.
(20) Kelton, K. F. Solid State Phys., 1991, 45, 75.
(21) Kelton, K. F.; Greer, A. L. Phys. Rev. B, 1988, 38, 10089.
(22) Gránásy, L.; Pusztai, T.; Warren, J. A.; Douglas, J. F.; Börzsönyi, T.; Ferreiro, V. Nature Mater., 2003, 2, 92.
(23) Kobayashi, R., Warren, J. A.; Carter, W. C. Physica D, 1998, 119, 415.
(24) Warren, J. A.; Gránásy, L.; Pusztai, T.; Börzsönyi, T.; Tegze, G.; Douglas, J. F. Proc. TMS Ann. Meeting, San Francisco, 2004, accepted for publication.
(25) Kvamme, B.; Tanaka, H. J. Phys. Chem., 1995, 99, 7114.
(26) Kvamme, B. unpublished.
(27) Stewart, P. B.; Munjal, P. J. Chem. Eng. Data, 1970, 15, 67.
(28) Kashchiev, D.; Firoozabadi, A. J. Cryst. Growth, 2002, 243, 476.
(29) Hardy, S. C. Philos. Mag., 1977, 35, 471.
(30) Anderson, R.; Llamedo, M.; Tohidi, B.; Burgass, P. W. J. Phys. Chem. B, 2003, 107, 3507.
(31) Pratt, R. M.; Mei, D.-H.; Guo, T.-M.; Sloan, E. D. J. Chem. Phys., 1997, 106, 4187.
(32) Teng, H.; Yamasaki, A. J. Chem. Eng. Data, 1998, 43, 2.
(33) Harris, J. G.; Yung, K. H. J. Phys. Chem., 1995, 99, 12021.
(34) Hoyt, J. J.; Asta, M.; Karma, A. Phys. Rev. Lett., 2001, 86, 5530.